CHAPTER 3

Experimental considerations

3.1 Introduction

In order to study the spectroscopy of molecular aggregates in the time domain, picosecond techniques must be used. The dephasing and fluorescence lifetimes range from 1 ps (picosecond) to about 500 ps. An excitation source with a pulse width of about 1 ps is necessary in order to resolve the dynamics of processes with the quoted lifetimes.

The main portion of the experimental work presented in this thesis has been done using a so–called synchronously pumped modelocked picosecond dye laser. Such a laser can routinely produce 3 to 4 ps pulses in most of the visible and near infra–red parts of the optical spectrum. The pulse from the laser is split into two parts that follow different optical paths. The two parts of the pulse are recombined in the sample, allowing for the detection of transient absorption changes. This pump/probe spectrometer uses the same design as Hesselink [1] in the first accumulated photon echo experiments [2]. Molenkamp [3] dedicated the apparatus fully to the generation and detection of accumulated echoes. The proposed changes to improve the detection sensitivity [3] have been applied, and have extended the sensitivity of the apparatus. The experimental complications of picosecond spectroscopy will be discussed in Sect. (3.2) through Sect. (3.4), along with a description of the measured nonlinear optical responses.

A modification of the laser and the addition of several electronics modules allowed us to do time correlated single photon counting experiments. This long established technique [4] has gained new impetus from the commercial availability of microchannel plate (MCP) photomultipliers with rise times as short as 100 ps. Combining these with appropriate fast electronics results in approximately 50 ps responses to ultrashort pulse excitation. The signal to noise ratio is determined by the number of detected fluorescent photons, and so just depends on collection time. The noise statistics follow a Poisson distribution, so the achievable extremely good signal to noise ratio allows for reliable data analysis by reconvolution fitting down to decay values of 10 ps. In Sect. (3.5) this technique is further explained.

In Sect. (3.6) the data collection and data analysis using microcomputers is described. The apparatus had already been automated in the past [3], using the first generally available microcomputer; the APPLE II. The need for more and faster data handling, together with reliability problems caused by the aging of the APPLE has made us discard this computer. The widely used IBM personal computer technology was chosen as replacement. New programs have been written both for data acquisition and analysis.

Sect. (3.7) and Sect. (3.8) describe the spectroscopical and chemical techniques that are used for the experiments. The preparation of aggregated samples of the dyes under study is rather delicate. Details concerning concentrations and cooling of the solutions can be found in the last section.

3.2 Pump/probe spectroscopy

3.2.1 Theoretical background

A block diagram of the transient absorption or pump/probe experiment is shown in Fig. (3.1). An intense pulse of light (partially) excites the sample. Considering the optical absorbers as a collection of a two level systems, the laser pulse induces the transfer of population from the electronic ground state to the excited state. Since the absorption coefficient is proportional to the population difference of the two levels, this implies that the absorption is reduced after the passage of the pump pulse through the sample. The reduction of the absorption is measured by the probe pulse that arrives after a variable delay.

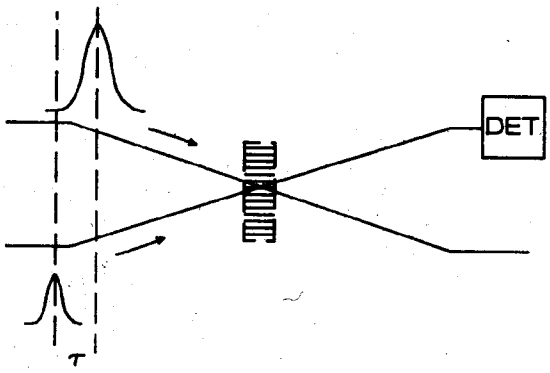

Figure 3.1 *Layout of the basic pump/probe experiment: the probe pulse reads the remaining sample absorption at time* τ *after the passage of the pump pulse. The change of the probe pulse transmission* ΔI *is recorded by the detector (DET).*

Ideally both pulses should have negligible duration compared with the dynamics under study, and have no relative timing jitter. These conditions cannot always be fulfilled. A more complete description of the induced absorption change [5] must be used:

$$\Delta\alpha(t_2) \propto \int dt_1 R(t_2 - t_1)\, I_{pump}(t_1) \quad . \tag{3.1}$$

Here $\alpha(t)$ is the absorption at time t, $I_{pump}(t)$ is the temporal profile of the pump pulse, and $R(t)$ is the molecule response function of interest. The change of transmission is measured by the probe pulse:

$$\ln(I/I_0) = -\alpha c l \tag{3.2}$$

and

$$\begin{aligned} \Delta(I^{\tau}_{probe}(t_2)) &= \Delta\alpha(t_2)\, I^{\tau}_{probe}(t_2)\, c l \\ &= \Delta\alpha(t_2)\, I_{probe}(t_2 - \tau)\, c l \quad , \end{aligned} \tag{3.3}$$

where τ is the time delay between pump and probe pulses. In all practical cases we follow ΔI as a function of τ. The dependence on t is integrated by the slow optical detector.

$$\begin{aligned}\Delta I_{probe}(\tau) &\propto \int dt_2\, \Delta\alpha(t_2)\, I_{probe}(t_2-\tau)\\ &= \iint dt_2 dt_1\, R(t_2-t_1)\, I_{pump}(t_1)\, I_{probe}(t_2-\tau)\\ &= \iint dt_1 dt_2\, R(t_1)\, I_{pump}(t_2-t_1)\, I_{probe}(t_2-\tau)\\ &= \int dt_1\, R(t_1) \int dt_2'\, I_{pump}(t_2'+\tau-t_1)\, I_{probe}(t_2')\\ &= \int dt_1\, R(t_1)\, G(\tau-t_1) \qquad (3.4)\end{aligned}$$

This result shows that the measured signal is the impulse response $R(t)$ of the chromophore, convoluted with the intensity correlation of the laser pulse $G(t)$.

In practical situations often only one laser is used. The output pulse is split in two parts, the weaker delayed part is used as probe, the stronger part is used as pump pulse.

$$I_{probe}(t) = q\, I_{pump}(t-\tau), \quad q<1 \qquad (3.5)$$

In addition to the coupling of the intensities of the pulses, also the coupling of the fields must be taken into account. This will result in the so called coherent artifact. The effect of the pulses has to be expressed in terms of the change of the third order nonlinear polarization [6]. The effect of three fields on a medium possessing a finite third order nonlinear polarizability is expressed as:

$$\begin{aligned}P_i^{(3)}(\mathbf{r},t) = \iiint dt_1 dt_2 dt_3\, \chi_{ijkl}^{(3)}(\mathbf{r},t-t_1,t-t_2,t-t_3) \times\\ E_j(\mathbf{r},t_1) E_k^*(\mathbf{r},t_2) E_l(\mathbf{r},t_3). \qquad (3.6)\end{aligned}$$

Here $\chi^{(3)}$ represents the time dependent nonlinear susceptibility tensor, and E is a component of the field $\mathcal{E}$ inducing the third order polarization change in $P^{(3)}$. The subscripts i,j,k,l refer to the axes of the spatial coordinate system. The time dependent $\chi^{(3)}$ tensor is a generalization of a frequency domain concept. It has been shown that this generalization is not without complications [7]. These complications are caused by the explicit time ordering of the interactions in a time dependent description. In a frequency domain description the permutations of all interactions have to be taken into account. Strictly speaking, the frequency domain and time domain description of the nonlinear susceptibility are not connected by a Fourier transform. For the description of pump/probe spectroscopy however, the third order nonlinear polarization as given in Eq. (3.6) is sufficient. Expressions for $\chi^{(3)}$ have been given [6] but these expressions are not amenable to computation because of the complexity of the large number of terms. The usual

approach is to isolate the relevant terms, without requiring knowledge of all of the resonances and damping parameters.

The first assumption is that the electric field $\mathcal{E}(\mathbf{r},t)$ is quasi monochromatic. The second assumption is that the field is incident in the form of a pulse that has a temporal profile that changes much more slowly than the inverse frequency of the field. This slowly varying envelope approximation (SVE) clearly holds in the case of picosecond pulses. In femtosecond nonlinear spectroscopy a breakdown of the approximation is expected; a 6 femtosecond pulse [8] in the visible part of the spectrum only consists of 3 optical cycles.

The expression for the field is:

$$\mathcal{E}(\mathbf{r},t) = \boldsymbol{E}(\mathbf{r},t)\exp(-i\omega t) \quad . \tag{3.7}$$

The time averaged intensity change of the probe now becomes:

$$\Delta I = \int dt \mathrm{Re}\left(\boldsymbol{E}^* \frac{\delta P^{(3)}}{\delta t}\right) \quad . \tag{3.8}$$

In case of pump/probe spectroscopy the relevant relaxation is the population relaxation. The phase relaxation that describes the loss of coherence by the ensemble of absorbers is considered to be very fast. In this limit the expression for the bleaching can be simplified, just using one response function $R(t)$ which describes the population decay,

$$\Delta I = \iint dt\, dt' E_i^*(\boldsymbol{r},t) E_j(\boldsymbol{r},t) R_{ijkl}(t-t') E_k^*(\boldsymbol{r},t') E_l(\boldsymbol{r},t') \quad . \tag{3.9}$$

In the pump/probe geometry in some cases the same source is used to generate both of the required pulses. The incident electric field is treated as a combination of plane waves with wavevectors $\boldsymbol{k}_{pump}$ and $\boldsymbol{k}_{probe}$.

$$E_{total}(\boldsymbol{r},t) = E_1(t)\exp(i\boldsymbol{k}_{pump}\cdot\boldsymbol{r}) + qE_1(t-\tau)\exp(i\boldsymbol{k}_{probe}\cdot\boldsymbol{r}) \tag{3.10}$$

Inserting a field of the form of Eq. (3.10) in the expression for the transmission change leads to:

$$\Delta I(\tau) = \iint dt dt' |E_1(t-\tau)|^2 R^{2211}(t-t') |E_1(t')|^2 + \iint dt dt' E_1^*(t-\tau) E_1(t) R^{2112}(t-t') E_1^*(t') E_1(t'-\tau) \quad . \tag{3.11}$$

The superscripts of the response function denote that a discrimination must be made concerning the time order of the interactions. R^{2211} denotes the response caused by an interaction of the form two times the pump field followed by two times the probe field. In this way the first part of Eq. (3.11) reproduces Eq. (3.4), and just gives the desired decay function convoluted with the intensity autocorrelation of the incident fields. The extra term is the result of an interaction where the pump and probe field coupled directly. It has the form of the field

autocorrelation and is called the "coherent artifact". It must be stressed that the coherent coupling of the field is not directly connected to dephasing of the optical oscillators. The source of the artifact is the absorption bleaching response $R(t)$, without dependence on the dephasing time. In experimental situations where the exciting laser pulses are not perfectly modelocked, the artifact appears as a spike at $\tau = 0$.

Before turning to the experimental realization of pump/probe experiments two more problems must be addressed: the stochastic field response and the depolarization behavior. An exactly transform limited pulse is characterized by the exact correspondence of intensity and electric field autocorrelation. Whether or not it is possible to make transform limited pulses depends on a number of experimental parameters like laser loss and gain, and cavity stability. In most cases the limit of perfect pulses will be not reached, and fluctuations in the optical fields will be unavoidable, giving rise to different field and intensity autocorrelation functions. These autocorrelation functions can be recorded by noncollinear second harmonic generation [14]. For example, in Fig. (3.2.c) a poorly modelocked pulse is shown ("Prussian helmet"), together with two traces showing better correspondence of field and intensity autocorrelation traces.

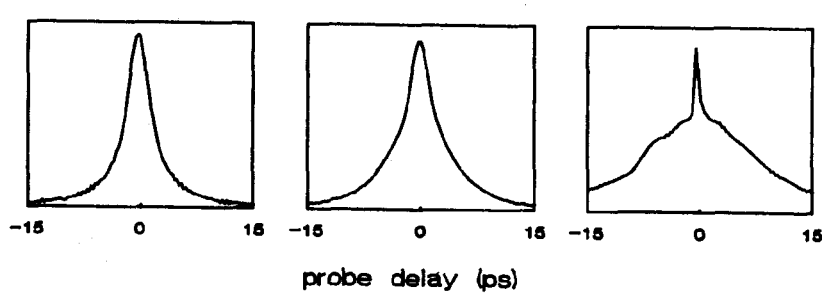

Figure 3.2*a*, *b* and *c* *Noncollinear autocorrelation traces of laser pulse from a synchronously pumped dye laser. In a) the pulse is nearly perfectly modelocked, in b) the autocorrelation trace starts to exhibit wings, indicating the presence of extra frequency components, in the pulse spectrum and in c) the autocorrelation consists of two easily discernible parts: a field and an intensity part.*

The spike in Fig. (3.2.c) is given by terms containing $|E^*(t)E(t-\tau)|^2$, and the background by terms containing $|I(t)I(t-\tau)|$. In recent publications the effect of extremely incoherent pulses was treated both theoretically and experimentally [9–12]. The field from the laser is treated as consisting of random field fluctuations as in a thermal source (stochastic fields). In some techniques that study dephasing this offers the advantage of increased time resolution, as for example the stochastic accumulated echo (Sect. (3.3)). Since the pump/probe technique relies on the intensity correlation (the background in Fig. (3.2c)) transform

limited pulses seem to be optimal. Morita has shown that this is not always true. For random fields Eq. (3.11) must be averaged over the fluctuations and turns into:

$$\begin{aligned}\Delta I(\tau) &= \iint dt dt' \langle E_1^*(t-\tau)E_1(t-\tau)\rangle R(t-t') \langle E_1^*(t')E_1(t')\rangle \\ &+ \iint dt dt' \langle E_1^*(t-\tau)E_1(t')\rangle R(t-t') \langle E_1^*(t')E_1(t-\tau)\rangle \\ &+ \iint dt dt' \langle E_1^*(t-\tau)E_1(t)\rangle R(t-t') \langle E_1^*(t')E_1(t'-\tau)\rangle \\ &+ \iint dt dt' \langle E_1^*(t-\tau)E_1(t'-\tau)\rangle R(t-t') \langle E_1^*(t')E_1(t)\rangle , \qquad (3.12)\end{aligned}$$

where the brackets denote the averaging. The first two terms in Eq. (3.12) originate from the intensity term in Eq. (3.11), the last terms derive from the coherent artifact term in Eq. (3.11). The first term is the background of the autocorrelation convoluted with the response and the third term is the coherent artifact. Next to these familiar terms two new ones are introduced that are caused by the fluctuating character of the fields. The fourth term is the coherent contribution that lasts for the total pulse time, and does not contain information about material dynamics. The second term contains dynamical information: it is the field cross–correlation convoluted with the decay function. When lasers are used that are very incoherent (pulse width τ_p much larger than the field correlation time τ_c), and the relevant dynamics are much faster than the pulse envelope, the second term leads to a decaying contribution to the coherent artifact. Since the correlation time τ_c of the pulses can be much shorter than the pulse time τ_p this can offer great advantages when studying fast dynamics. One important drawback however must be noted: the relative intensities of the coherent spike (term 3) and the decaying part (term 2) are determined by the ratio of the decay time of R and the correlation time of the fluctuating field τ_c. To obtain reliable results the correlation time must be about a factor of three shorter than the decay time. This requires knowledge of the time scale of the dynamics before doing the experiment. Better applications of stochastic fields will be treated in Sect. (3.3).

When polarized laser light is used, the interpretation of pump/probe data is more complicated [13]. Exciting an ensemble of chromophores with a polarized laser pulse will induce an anisotropy in the absorption profile. The chromophores that have transition moments aligned parallel to the polarization of the field will have the greatest probability of getting excited. The ones that have perpendicular transition moments will not be excited at all. Probing this anisotropic excitation with polarized light will only give the desired decay response, as long as the directions of the transition moments do not change during the measuring period. In general the molecule and/or the electron distribution do change position. Studying the depolarization provides relevant information about the interaction of the chromophore and its environment. A method is needed to separate the depolarization response $\rho(t)$ from the excited state decay response $R(t)$.

Consider an ensemble of molecules partially excited by a x-polarized pump pulse. The molecules are randomly oriented, but x-polarized light will be absorbed preferentially by those molecules having their transition moments oriented in the x-direction. A non-random distribution of orientations of the excited molecules will be the result. The excited molecules will relax to the ground state according to $R(t)$, and the distribution of excitation will change according to $\rho(t)$. The decay response $R(t)$ is of the form:

$$R(t) \propto N_x^{ex}(t) + N_y^{ex}(t) + N_x^{ex}(t)$$
$$= N_{\parallel}^{ex}(t) + 2N_{\perp}^{ex}(t) \quad . \tag{3.13}$$

Here $N^{ex}(t)$ is the time-dependent excited state population projected on one of the Cartesian axes. Probing the sample with light polarized parallel and perpendicular to the pump implies detecting $N_{\parallel}$ and $N_{\perp}$ respectively. $R(t)$ can be recovered by adding them according to Eq. (3.13). Another possibility is to choose the relative angle between pump and probe in such a way that the terms are measured in a weight according to Eq. (3.13). This magic angle can be found when one realizes that the parallel excitation is proportional to the cosine squared of the angle between polarization and transition vectors, whereas the perpendicular excitation is proportional to the sine squared. Now the probe must detect the contributions in the weight 1:2, this implies $\cos^2(\alpha)/\sin^2(\alpha) = 1/2$; $\alpha = 54.7^o$.

In addition to measuring the pure decay function function it is also possible to measure the pure orientational relaxation $\rho(t)$,

$$\rho(t) = \frac{N_{\parallel}^{ex}(t) - N_{\perp}^{ex}(t)}{N_{\parallel}^{ex}(t) + 2N_{\perp}^{ex}(t)} \quad . \tag{3.14}$$

Here the difference in parallel and perpendicular excited state population is normalized to the total excited state population. In the case where the transition moment is fixed in space, as in a low temperature glass, $\rho(t)$ has the value 2/5 (because of isotropic symmetry the ratio $N_{\parallel}$ to $N_{\perp}$ is 3). If the transition moment can change its spatial direction $\rho(t)$ decreases from 2/5 to 0. Even if the molecule is fixed in a matrix $\rho(t)$ can change because of electronic redistribution over the molecule, or transfer of excitation to other molecules.

3.2.2 Experimental setup

Fig. (3.1) shows that a pair of pulses, having pulse lengths that are short compared to the dynamical constants under study with an adjustable optical delay, is required to perform a pump/probe experiment. In order to produce pulses of less than a nanosecond, one relies on mode locking techniques [14]. In a modelocked laser the balance of gain and loss is varied periodically, which lead to pulse formation. The variation of the gain is achieved either by an optical modulator in the cavity (active

modelocking) or a saturable absorber in the cavity (passive modelocking). In the work presented here the first method is used. In a modelocked argon laser ionized argon gas is the gain medium, and an acousto–optic modulator is the loss device. The modulator "opens" at a frequency which is exactly the inverse of the round trip time, $\nu = c/2L$, where c is the speed of light in the medium and L is the length of the cavity. The match of the modulation frequency to the inverse round trip time enables repetitive amplification of a pulse after one or more round trips. The output of the laser consists of a continuous train of pulses with a width of approximately 100 ps, and with a repetition rate of about 94.4 MHz. The length of the dye laser is matched to the length of the pump–laser in order to benefit once more from synchronous gain modulation by repetitive amplification. This synchronous pumping scheme ("sync pump dye laser") can produce wavelength tunable pulses shorter than one picosecond. In Table (3.1) the laser system is specified.

Table 3.1 Picosecond laser system

laser–type	O/C[(a)]	λ	power	pulse
Ar–ion Coherent Innova 99	12 %	514.5nm	600mW at 45 Amp	75 ps
dye laser Coherent 590/599	10%–35%	525–1000nm	50–150mW	2–5 ps

(a) output coupling percentage

The argon laser was modified to match the length imposed by the available modelocking crystal. A new output coupler assembly was made and inserted in the cavity, and the modelocking crystal holder was mounted on the end plate.

Different laser dyes have to be used to cover the whole wavelength range cited in Table (3.1). The optimal concentration of dye is determined by the absorption coefficient of the dye. The absorption in the dye jet is increased to 90%, by increasing the dye concentration while monitoring the transmission of the pump light through the jet [15]. The output coupling percentage of the dye laser is chosen as high as possible, still meeting minimum power requirements (stable operation is possible above 10 mW). High output coupling turns out to be the key parameter for good short pulse performance. A wide variety of partially transmitting optics was used: Ar– and Kr–laser mirrors, and many different dye laser mirrors. Some of these are planar, other ones are curved, but that does not cause optimization problems [16]. The output coupler is selected by a trial and error substitution procedure.

In Fig. (3.3) the complete experimental apparatus is shown. The output beam of the dye laser, consisting of a 94.4 MHz pulse train, is split in two beams by a beam splitter. The experiments on TPY–aggregates (Chapter 6) were done with two dye lasers at different wavelengths (50% of the pump beam was sent into another dye laser parallel to the one in Fig. (3.3)). One of the two beams passes a variable delay (MD) consisting

of a retro–reflector on a cart, which can be moved on a rail. The precision of the translation is 1.5 μm. Since light travels 0.3 mm in 1 picosecond, moving a few cm generally is sufficient for scanning the time range of interest. Behind the sample the pump beam is blocked, and the probe transmission is monitored. This optical design allows for simultaneous detection of signal and pulse characteristics. Knowing the particular pulse autocorrelation associated with an experiment reduces the uncertainty in the fitting procedure.

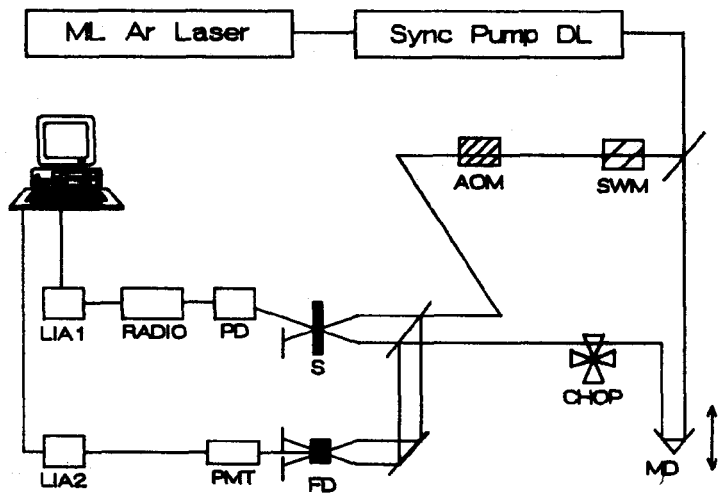

Figure 3.3 Picosecond pump/probe and accumulated echo setup. The output of the dye laser is split into pump and probe beams, and recombined in the sample (s) and a frequency doubling crystal (FD). The signal and the autocorrelation are demodulated simultaneously, and the traces are stored in a microcomputer.

The low peak power, high repetition rate pulses induce only small (10^{-6} to 10^{-5}) relative transmission changes. The quasi–continuous character of the beams however, allows for the use of sophisticated modulation techniques. In our pump/probe experiments the probe beam is modulated at audio frequencies (100 Hz to 500 Hz) by a mechanical light chopper (PAR 191, CHOP in Fig. (3.3)). The pump beam is modulated at a radio frequency (20.060 MHz), by a standing wave modulator (SWM, Intra–action SWM 102). Since the bleaching signal is proportional to the product of pump and probe intensities, modulated at 200 Hz and 20 MHz respectively, the signal will be modulated at 20 MHz $\pm$ 200 Hz.

A low noise silicon p-i-n diode (EGG SGD100) detects the change of the transmission. The electrical output is filtered and amplified, and fed into a radio (Drake R7) that handles the electrical signal the same way as AM antenna input. The output of the radio is a 200 Hz audio signal, which can actually be heard from the speaker. The low frequency is demodulated by a lock–in amplifier (LIA, EGG PAR 128A), and the resulting DC signal is fed into the microcomputer. The photomultiplier (PMT)

response is too slow to detect the 20 MHz modulation. Actually, it is not the PMT itself but the load network of the PMT that limits the time response. The output is fed directly into another lock-in, without high frequency demodulation. The benefit of this complicated modulation scheme is the use of the gap in the noise spectrum in the frequency band from 3 MHz to 30 MHz in modelocked dye lasers [17]. The minimum detectable signal modulation, $\Delta I/I$, can be as low as 10^{-8} compared to 5×10^{-4} [3] in the apparatus that did not use high frequency modulation. In Sect. (3.4) more details will be given on the operational principles of the radio detection.

When the same laser is used for the generation of both pump and probe, an extra acousto-optic modulator (AOM, SORO) is used. This device launches a *travelling* wave into a crystal. Scattering a laser pulse from the travelling refractive index grating gives rise to a phase shift of the light. Since the driving frequency is not slaved to the modelocking frequency, the relative phase shift for consecutive pulses is essentially random. Grating accumulation can no longer occur: the signal is "clean", not buried in large accumulated coherent artifacts. I refer to Sect. (3.3) for further details.

3.3 Photon echoes

3.3.1 Stochastic accumulated echoes

In the treatment of pump/probe spectroscopy in the previous section, it was stated that the absorbers were assumed to have no phase memory (or equivalently $T_2=0$). When this condition does not hold, other third order nonlinear effects can occur. The particular kind of nonlinear phenomenon used most frequently for the work presented in this thesis is the photon echo. The use of photon echoes for the determination of dephasing times has been fruitful [18–20]. Especially the accumulated photon echo has proved to be a relatively simple and reliable technique for the study of the dephasing of chromophores in various solid environments [3].

Photon echo spectroscopy gives information about the homogeneous optical lineshape of chromophores. For chromophores in solid environments the observed linewidth can be separated into three components. The first contribution can be assigned to the lifetime of the excited state (T_1), which may be converted into a linewidth via the uncertainty relation $\Delta E\Delta\tau>\hbar$. The second contribution is caused by the dephasing (T_2) of the ensemble of absorbers. These first two terms generally lead to Lorentzian contributions to the total linewidth. The last term is the inhomogeneity. It represents the spread of the transition energies of the absorbers caused by the different local environments for the different absorbers. Since inhomogeneity is caused by statistical spread of single molecule energies, the inhomogeneous contribution is generally considered to lead to a Gaussian distribution of the transition frequencies.

When two pulses in the pump/probe geometry (Fig. (3.1)) are combined with zero time delay, interference of the fields leads to a grating. Both fields are identical except for a wavevector difference of $\mathbf{k}_{pump}-\mathbf{k}_{probe}$, which is exactly the difference that characterizes the intensity grating.

A sample placed in this spatial grating will be excited at the positions of the maxima, and consequently an absorption grating in the sample will be formed. When the two fields are given a relative time delay, the grating formation will depend on the value of the dephasing time. Very rapid dephasing ($T_2 \ll \tau_c$, where τ_c is the electric field correlation time) will lead to a response which is limited by the field correlation time, and is related to the coherent artifact discussed in Sect. (3.2). In the opposite limit of no dephasing the situation is more complex. After application of the first field the individual absorbers will oscillate collectively. Because of the fact that the oscillators have different inhomogeneous offset frequencies Δ, inhomogeneous dephasing will occur. The interaction of the second field incident with the oscillators will now lead to formation of a grating which is dependent on both the wavevector difference and the inhomogeneous offset [1]:

$$p \propto \exp(-\tau/T_2)\cos(\Delta\tau - \Delta\mathbf{k}\cdot\mathbf{r} + \phi_{12}) \quad . \tag{3.15}$$

Here p is the excitation parameter, proportional to the population difference of the ground and excited states after the application of the two excitation fields. The oscillatory term both contains a frequency grating term ($\Delta\tau$), and a spatial grating term ($\Delta\mathbf{k}\cdot\mathbf{r}$). Analogous to light scattering from a spatial grating, scattering can also occur from the frequency grating, giving rise to time delayed scattering: the photon echo.

It is important to realize that the grating formation depends on the correlation of the fields and not on the correlation of the intensities [21,22]. Interference of optical fields occurs within the coherence time of the fields. Some years ago it was shown independently by Hartmann [11] and Morita [10] that photon echoes can be generated with incoherent sources. They were the first to use the correlation time of exciting source, and their work formed the basis for other variants of correlation spectroscopy.

Accumulated photon echoes are a result of the formation of a population grating described by Eq. (3.15). The salient feature of the accumulated echo is the build-up of the grating by many pulse pairs. The build-up is possible as long as the decay of the grating is slower than the repetition time of the pulses. In Fig. (3.4) the sequence of pulses is shown. The repetition rate is determined by the modelocking frequency of the laser (94.4 MHz, 10.2 ns pulse separation). When the ground state recovery is faster than 10 ns, as in most dye molecules, no accumulation can take place. In a large number of different molecules however, intersystem crossing to a triplet state can take place. The population grating of the excited state decays to some extent (determined by the intersystem crossing yield) into that triplet state. Only the grating in the ground state remains, but that is sufficient to generate an echo signal.

From the accumulated grating, echoes are generated by the pump pulse of the next cycle of the laser, as indicated in Fig. (3.4). The echo generated has the same wavevector as the probe pulse and is exactly time coincident with that probe pulse. Now as in the case of pump/probe experiments, the polarization interacts with the field, leading to an

intensity change as in Eq. (3.8). This process was named heterodyne beating, after the use of that term in radio technology. However, heterodyne beating refers to mixing a signal at frequency ω_1 with a carrier at frequency ω_2 and consequently detecting the beat frequency $\omega_1 \pm \omega_2$. In the sense of creating an interference of the third order nonlinear polarization $P^{(3)}$ at frequency ω with the probe field E also at ω, it is better to use the term homodyne detection.

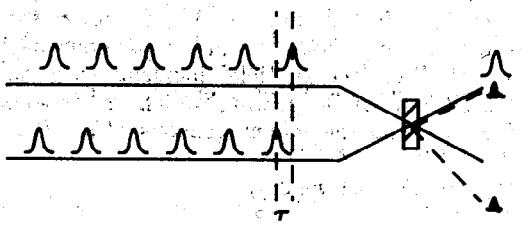

Figure 3.4 The accumulated echo sequence is a continuous repetition of the pump/probe sequence. When the dephasing time T_2 is larger than the pulse length and a long lived bottleneck exists, an accumulated photon echo is generated. The wavevectors of the pulses must be matched, which leads to two distinguishable echo directions. The downward direction corresponds to the side scattered echo (proportional to P^2) and the upward direction corresponds to the homodyne echo ($\propto P \times E$).

The accumulation of the grating is governed by the correlation of the optical fields, so the time resolution in the measurement is determined by the field correlation time τ_c. In other nonlinear optical techniques that depend on the field correlation such as self–diffraction or CARS, interfering signals exist that are caused by contributions from the intensity correlation. In the case of accumulated echoes the long period between grating generating pulse pairs leads to a decay of all populations and coherences, and the only remaining contribution is the grating that was generated during the time interval τ. The accumulated echo is one of the few cases that allow for the use of correlation spectroscopy without introducing new ambiguities in the signal characteristics.

The experiment is performed according exactly to the scheme which was outlined in Sect. (3.2.2) for pump/probe spectroscopy. The echo has exactly the same wavevector as the probe pulse, and the signal is detected as a change in the probe transmission. The discrimination between pump/probe and echo signals is made on the basis of the response to incoherent excitation; in that case the pump/probe signal grows with the intensity correlation (the broad background in Fig. (3.2c)), whereas the echo grows with the field correlation (the spike in Fig. (3.2c)).

3.3.2 Acousto-Optic Modulator effects

In Sect. (3.2) I stated that a travelling wave modulator scrambles the

phase of light fields, and is used to discriminate accumulated from single pulse events. I will show why a standing wave modulator can be used for modulation of accumulated photon echo signals and a travelling wave modulator cannot.

An acousto–optic modulator is a piece of glass or quartz brought into oscillation by a transducer. A sinusodal voltage is applied to this transducer. Longitudinal compression waves are sent into the material, where they form a grating in the index of refraction. An light wave that is incident on the grating will diffract. In Fig. (3.5) the situation is depicted; only the maxima of the grating are indicated.

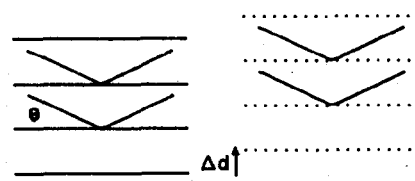

Figure 3.5 *A light wave is incident at a Bragg angle θ_B. Between the arrival of the pulses the grating moves a distance Δd, this shift is directly converted into a change of the relative phase difference ϕ_{12} by an amount $\Delta d/\Lambda$.*

Diffraction only occurs at a specific angle, the Bragg angle, which is defined by:

$$2\Lambda_{acoust}\sin(\theta_B) = \lambda_{light} \quad . \tag{3.16}$$

In Eq. (3.16) Λ_{acoust} is the wavelength of the index grating and is given by the speed of sound divided by the driving frequency. The reflections from planes that are one acoustic wavelength apart have a phase difference of 2π. If the maxima of the index grating shift by a distance Δd, the phase of the light will shift by an amount $\Delta d/\Lambda$. A travelling acoustic wave thus gives rise to a time dependent phase shift of the light [23]:

$$\Delta\Phi(t) = 2\pi/T_{acoust} \times \Delta t = \omega_{acoust} \times \Delta t \quad . \tag{3.17}$$

An alternative way of stating this is that the frequency of the travelling wave is added to the optical frequency, which means that the optical frequency of the diffracted light is shifted by an amount ν_{acoust}. For a standing wave modulator no time dependent phase shift occurs since the maxima of a standing wave are fixed at a position in space.

The time dependent phase shifting of the light has consequences for the pump/probe spectrometer of Fig. (3.3). The picosecond pulse is split, so the probe is an image of the pump. The pump pulse is diffracted in the travelling wave modulator TWM. The pulse lasts only for picoseconds, so the travelling grating is "frozen" at a particular Φ, and the pump pulse

is phase-shifted by that amount. Focusing the pump and probe in the sample implies that the experiment is done with a relative phase difference $\Delta\Phi$. For a pump/probe experiment this phase difference poses no problem; the probe can be delayed relative to the pump by many picoseconds, or thousands of optical cycles. A phase shift of π only implies an extra delay of 1 femtosecond. A similar argument shows that the two pulse echo is also not affected.

The accumulated echo experiment however, is seriously disturbed by this phase shifting. For accumulation to occur, the grating term of Eq. (3.15) must be constant during the preparation period. That is, the relative phases of the pump and probe must be constant during the full accumulation period. However, we saw that the phase of the pump pulse is modulated by the driving frequency of the travelling wave modulator. For example the pulses have a repetition frequency of 94.4 MHz and the modulator is driven at 200 MHz. This implies a phase shift between consecutive pump pulses of $(200/94)\times 2\pi$ is 4.2373π. Since this clearly is not a multiple of 2π, the accumulation efficiency will be strongly reduced.

The inhibition of accumulation by a travelling wave modulator was discovered by Hesselink [1]. The increase in signal sensitivity by application of high frequency modulation allows for the parallel detection of single pulse effects and accumulated effects, without the need for amplifying the laser pulses. The inhibition of accumulation by a travelling wave modulator can be used for the clear discrimination of the different effects.

3.4 High frequency modulated detection

The main improvement of the accumulated echo setup relative the old situation [3], was the application of high frequency modulation techniques [24–27]. I will discuss why high frequency modulation is so helpful, and I will explain a few technological radio tricks. For a thorough discussion of the modulation and detection scheme I refer to the work of van Exter [28]

Accumulated echo spectroscopy is a nonlinear technique with a signal strength that is proportional to the square of the applied intensities ($S = I^2$). When the intensities fluctuate by a certain fraction, the signal strength will fluctuate approximately twice as much ($\Delta S/S = 2\,\Delta I/I$). This fact imposes the need for stable lasers and sensitive detection. The signal is measured on a large background of the probe intensity, so lock-in detection is the method of choice. Detecting with a lock-in amplifier is done by modulating the signal component at a frequency ν_{mod} and not the background, the small (AC) signal component is amplified by the lock-in. Narrow band filtering around ν_{mod} assures that only the noise in the frequency band around ν_{mod} is detected along with the detected signal.

The simplest way is to modulate the pump beam at ν_1 and the cross modulation of the probe intensity is detected. The major disadvantage of this approach is that any scattered light from the pump beam is indistinguishable from the signal. Modulating the probe beam as well, at

a different frequency ν_2, offers the opportunity to detect the signal term at frequencies $\nu_1 \pm \nu_2$. The scattered light from the pump beam is modulated at ν_1 and can be filtered out by the lock-in amplifier. The double modulation scheme can easily be realized by double light choppers which include all necessary frequency mixing electronics. Double modulation allows for stray-light free detection; the noise level is limited by the laser noise in the bandwidth around the signal modulation frequency $\nu_1 \pm \nu_2$.

The only choice that has to be made are the actual modulation frequencies. It is clear that the lowest possible noise in the signal is found at a frequency where the laser noise is at a minimum. Baer and Smith [17] measured the noise spectrum of a modelocked picosecond dye laser pumped by an Ar-ion laser, and found that there are many acoustic disturbances at low frequencies (Hz to kHz). The noise intensity gradually decreases at higher frequencies and reaches the so called shot-noise limit at 3 MHz. This shot-noise limit is reached when the noise is the result of the quantum statistics of the light: the fluctuation in the number of photons is the root of the total number of photons. The noise level stays low until 40 MHz, being the modelocking frequency of the dye laser. The conclusion is that the best choice is to modulate the signal at a frequency between 3 MHz and 30 MHz.

A number of schemes have been proposed to realize the double high frequency modulation [24–27]. The problem was the detection of small signals modulated at MHz frequencies. A simple lock-in amplifier does not work above 100 kHz, and a high frequency lock-in is expensive. The use of a commercial long distance (DX) radio overcomes this problem [28]. The first design used single side band demodulation. This demodulation implies that the radio is tuned to the carrier frequency (20 MHz) and demodulates the audio frequency (200 Hz). In this design, the internal oscillator has to be disconnected and an external carrier has to be supplied. A more simple way is to use amplitude demodulation (AM detection). In the AM mode the signal input is split in two parts, one of which is amplified until saturation. The saturated signal is used as a carrier wave, so frequency locking is always guaranteed.

The effectiveness of the radio detection approach is illustrated by the fact that the intensity stabilizer used previously in the optical apparatus could be discarded. In the old modulation scheme with just one light chopper, the stabilizer was essential to detect signals of about one part in thousand relative to the probe intensity. In the new high frequency modulation scheme detection of signal strengths of one part to ten million is achievable. One must realize that since the signal intensity is the product of pump and probe intensities the probe noise at 200 Hz will still be present in the signal. However, the noise must be evaluated relative to the signal strength: the signal is as stable as the laser. In the old modulation scheme, where the noise of the whole probe intensity was detected. The noise in the large nonmodulated background already exceeded the signal at the quoted signal strength of one part in thousand.

In Fig. (3.6) the detection electronics have been drawn schematically. The photodiode is part of a resonance loop, in order to increase the load of the diode. A diode is a current source, so the load has to be as large

as possible without limiting the frequency response. The 50 ohm input impedance of the amplifier is increased to 600 ohm, so a twelve fold increase in signal is achieved relative to direct input in the amplifier. A high quality preamplifier is used to match signal levels to the radio sensitivity. A small amount of carrier wave is added to linearize the response of the radio. The radio demodulates the 20 MHz carrier wave and the resulting 200 Hz signal is detected by the lock-in amplifier.

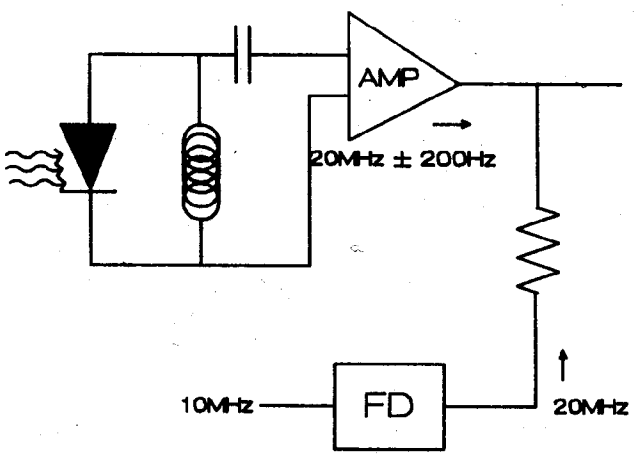

Figure 3.6 *Schematic representation of the electronics necessary to detect the high frequency modulated signal. The photocurrent generated in the photodiode is fed through a resonance loop consisting of a coil, a capacitor and the input impedance of the amplifier* [28]. *A small portion of the modulator driving frequency is fed in a frequency doubler (FD) that provides the unmodulated carrier necessary for the demodulation by the radio.*

In the case of pump/probe experiments the improvement is obvious, but a few remarks concerning the detection of accumulated echo signals must be made. A serious complication in the detection of accumulated echoes is the incoherent accumulated bleaching caused by bottleneck filling, leading to a bleaching not dependent on the time delay between the pulses. This effect always accompanies the accumulation [1] and gives rise to a constant background in the signal detection. Molenkamp [3] proposed to use an intricate four beam design to separate the background from the signal. He reasoned that the extra complication of the optical design would be compensated by increased signal to noise. When I installed the high frequency modulation it turned out that the extra beams were obsolete. The reason for this fact is the slow dynamics of the bottleneck, which is not modulated at 20 MHz, because the dynamics occurs at millisecond to microsecond time scales. All detection electronics are only sensitive at 20 MHz so no bottleneck effect is observed.

To summarize the advantages of high frequency modulated detection:
1) improved sensitivity for pump/probe spectroscopy,

2) laser intensity stabilization is rendered obsolete,
3) the saturated background of the accumulated echo is not detected.

3.5 Time correlated single photon counting (TCSPC)

The radiative lifetime of allowed transitions of dye molecules is several nanoseconds; for example, Rhodamine–6G has a decay time of 3 ns [13]. Rhodamine–6G has a high quantum yield for emission so the fluorescence decay is almost the same as the radiative lifetime. For other dye molecules with comparable radiative lifetimes the quantum yield is smaller than 1, and consequently the fluorescence lifetime is shorter than the radiative lifetime,

$$\tau_{fluor} = \tau_{rad}\,\phi, \quad \phi \leq 1 \quad , \tag{3.18}$$

where ϕ is the quantum yield for emission. Aggregate excitations show fluorescence lifetimes considerably shorter than the monomer radiative lifetimes, because of radiative coupling (Sect. (2.2)). In order to obtain reliable results on radiative dynamics a time resolved experiment must be performed.

Three ways to achieve the resolution needed are: direct detection, fluorescence upconversion [29–31] , and photon counting [4]. Direct detection of fluorescence implies monitoring the response of a fast photodiode or a streak camera which is illuminated by the fluorescence. The resolution is limited by the speed of the detector and can be less than 5 ps. Fluorescence upconversion uses a part of the exciting laser pulse to gate the emission. The gating pulse is delayed relative to the exciting pulse. The emission and the delayed gating pulse are focused in a nonlinear crystal, and the upconverted fluorescence is detected. Scanning the delay gives the desired fluorescence curve. The resolution is only limited by the pulse length of the exciting laser, so even femtosecond resolution is possible [31]. I used the third method: time resolved photon counting. The time interval between the exciting pulse and the emitted photon is measured very accurately (within 10 picoseconds). Repeating this "single photon experiment" many times gives the statistical distribution of arrival times. This distribution is just the decay function.

The advantage of the TCSPC technique is the use of very low light levels, less than one emitted photon per exciting pulse is sufficient. The signal to noise ratio is only limited by the statistics of the photons, and longer photon collection times give better signal to noise. The other two detection techniques need many more emitted photons, on the order of 10^9 (0.1 nJ in the visible range of the spectrum). Strong exciting pulses are needed. The signal to noise ratio is rather poor, since pulse to pulse intensity fluctuations cannot be avoided. In one case though the upconversion technique is superior; when the decay is shorter than 10 ps upconversion is the only reliable technique.

The recent availability of ultrafast photomultipliers has extended the possibilities of TCSPC. In these photomultipliers the electron avalanche occurs in short channels, which are only microns wide. The resulting

electron pulse is much shorter than that of the conventional design, because of the smaller spread in transit times. The risetime of the used Hamamatsu microchannel plate (MCP) is 190 ps. With the help of a constant fraction discriminator the triggering can be precise to 50 ps. The apparatus is shown in Fig. (3.7).

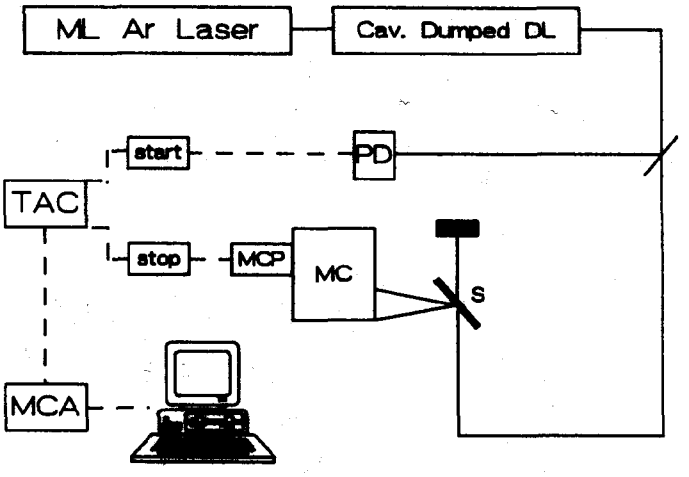

Figure 3.7 Basic time correlated single photon counting setup [34,35]. The dye laser is equipped with a cavity dumper that lowers the repetition rate of the pulses. The pulse is split into a trigger pulse for the diode (PD), and an exciting pulse that is focused in the sample. A monochromator removes unwanted resonant scattering, and the photons are detected by a microchannel plate (MCP). The time difference of the electronic pulses (indicated by dashed lines) is measured by the combination of a time to amplitude converter (TAC) and a multichannel analyzer (MCA).

The laser system consists of a modelocked argon–ion laser which pumps a synchronously pumped dye laser. The repetition frequency of the dye laser is lowered by a Spectra Physics 452 cavity dumper. This device allows for the build–up of high intra cavity power levels. Every N–th pulse that passes is deflected out of the cavity, where N is an integer from the series 20, 100, 200, 1000, et cetera. The lowering of the laser pulse repetition rate is necessary in order to prevent pile–up effects in the electronics. The output of the laser is split into a trigger pulse directed to a fast photodiode (Telefunken BPW28), and an exciting pulse directed to the sample (S). The fluorescent emission is collected either under a 90 degree angle as shown, or along with the exciting beam. A color filter absorbs the scattered laser light. The emission is directed through a grating monochromator (Jarrell–Ash 0.5 m), that serves to filter out the unwanted spectral area. A grating monochromator should have low dispersion in order to avoid unwanted transit time spread [32].

The fluorescence is diffused at the output slit by a roughened glass plate and hits the photocathode of the MCP (Hamamatsu R1564U–01 [34]).

The photocathode is sensitive at wavelengths from 350 nm to 850 nm. The anode pulse lasts for half a nanosecond and has a peak voltage of 10 mV. The constant fraction discriminator needs a pulse of a least 100 mV, so amplification is needed. Two cascaded broad band amplifiers are used (Mini–Circuits ZFL–2000). The amplification bandwidth is 10 MHz to 2 GHz in order not to loose any Fourier components of the signal. These Fourier components stretch this range because of the low repetition frequency of the photons on one hand, and the steep flanks of the pulses on the other hand. The amplified pulse is fed into one of the units of the quadruple constant fraction discriminator (Tennelec 455). The discriminator is needed to circumvent triggering problems associated with pulse height variations. The photodiode pulse is fed into another unit of the discriminator. The time difference between the two output pulses of the discriminator now contains the relevant information about the arrival time of the fluorescent photon after the excitation by the laser pulse.

Depending on the emission yield one counts either forward or reverse. Forward counting implies using the diode pulse as a start trigger, reverse implies starting on the emitted photon. The last way offers a higher collection efficiency at the cost of a reduction of the signal to noise ratio. The cavity dumper can be operated now at 4.7 MHz instead of 94 kHz in the forward mode. The two limits are set by the input characteristics of the discriminator and the time to amplitude converter.

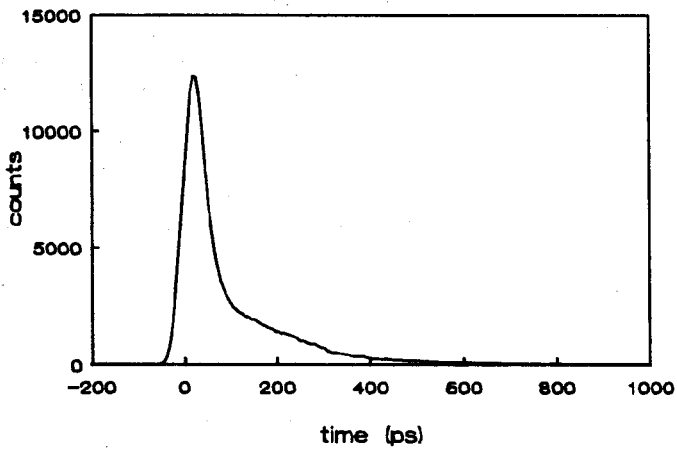

Figure 3.8 *Instrument response function with a width of* 75 *ps, measured from scattered laser light. The trigger pulses* (94 *kHz*) *preceded the photon pulses ("forward counting"). The width is reduced to* 45 *ps when a prism monochromator is used instead of a grating monochromator.*

The time difference is accurately converted into a pulse height by a time to amplitude converter (Ortec 457 TAC). The pulse height is measured by an analog to digital converter. Coupled to the TAC is a buffer that increments the proper memory position (Ortec 917 multi channel buffer). The electronics can work without the computer, which can even be switched off during the collection time. The advantage of the stand alone multi channel analyzer over the computer plug–in boards is evident; the

apparatus is more mobile, and computer failure does not destroy data. The main task of the computer is the graphic representation of the data, provided in scaled form by the micro-processor of the buffer.

The result of this elaborate scheme is shown in Fig. (3.8). Here the so called instrument response is shown. This is the response of the detection system to a laser pulse that has a width of a 5 ps. If fluorescence is detected, this response is convolved with the decay function. The instrument response function shows a tail caused by imperfect operation of the cavity dumper. The laser pulses vary in intensity, and this variation is detected by the fast photodiode. The width of the instrument response is less than 50 ps [35] without monochromator. The experiments quoted in this thesis were performed with the grating monochromator, where the response lengthens to 70 ps. The use of a prism monochromator and further optimization [36], recently improved the width of the system response to about 45 ps. The resolution of decay parameters can be a factor of five better because the noise in the data is only statistical. Fast decays can be fitted in a convolute and compare procedure, provided the signal to noise ratio is high enough.

3.6 Computer control and analysis

Experimental research is no longer done without support from automated equipment. Large amounts of data must be acquired, represented and fitted. The ideal situation would be that representation and fitting can be performed during data acquisition, and no time is lost on trivial data handling.

Great progress in the achievements of personal computers was made in the last decade. The APPLE-II computer that was operating the set-up in the past [3] has been replaced by a more powerful IBM PC/AT compatible computer. A slight change has been made in the way the computer is connected to the setup. No home built interfaces are used inside the computer anymore, as it turned out that these interfaces were the main source of problems in the APPLE-II. This choice was made easy by the availability of cheap standard interface cards. The necessary connecting electronics are mounted in a separate box. In Fig. (3.9) basic scheme is shown.

The input/output card (I/O) handles all digital information, such as pulses to the delay stage and inputs from a digital counter. The analog to digital converter (ADC) card reads the output of the lock-in amplifiers. The serial interface finally (RS232), connects to modern measuring devices that have some form of microprocessor control themselves, such as the multichannel buffer.

New software to use the possibilities offered by the large increase in computing power was written in our group [37]. The main part of the software consists of a new operating system shell, that is completely managed by pull down menus. Within this environment relatively small subroutines perform the specific tasks associated with a particular experiment [37].

Three programs must be mentioned: STAP, MCA and RAMAN. The first program controls pump/probe and accumulated echo experiments. It moves

the mechanical delay, and it stores the values from the lock-in amplifiers. The operation of the stepper motor is well developed. The backlash is compensated, and acceleration and speed can be adjusted. The collected signal traces together with experimental information can be stored on disc in the form of text files. The MCA program emulates a standard multi channel analyzer, and includes features like automatic scaling and automatic timing. Commercially available MCA programs are mostly specialized on nuclear experiments, instead of time resolved fluorescence. This fact makes the program better than commercial ones for this application. The RAMAN program scans a monochromator linearly either in wavelength or wavenumber. At the same time it reads the counter that monitors the number of Raman (or fluorescent) photons. These three programs allow for total digital storage of all data. However, in practice X-Y chart recorders were frequently used in steady state emission and absorption spectroscopy.

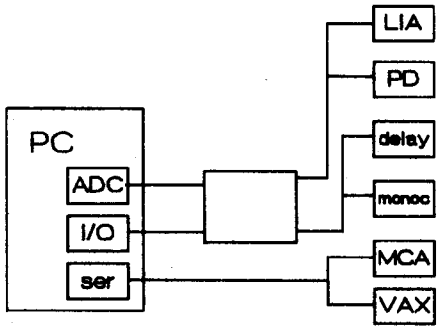

Figure 3.9 *Connections of the personal computer to the peripherals. The serial interface is connected directly to the measurement equipment, whereas some extra electronics is necessary for the ADC and I/O cards.*

An attached printer prints the experimental traces and relevant settings on a sheet of paper, so the data are directly accessible. It is also possible to process the traces to make them of presentation quality (vide infra).

Fitting data both has been done both on a VAX 11/750 computer, which is connected to the PC via a serial link, and on the PC itself. Because the echo decays of PIC aggregates turned out to be nonexponential, the standard linear least squares fitting procedures did not work [38]. The fluorescence decay data from the photon counting must be analyzed by reconvolution, which is not possible in "normal" least squares fitting. This limitation was overcome by implementing a nonlinear least squares fitting method using the Marqhart-Levenberg algorithm [39,40] . Arbitrary functions can be used in this iterative method. Reconvolution fitting of (multi) exponential as opposed to non-exponential decays was performed by the method outlined by Grinvald [41]. The algorithm is very efficient: when one starts with reasonable starting values four or five iterations generally suffice.

3.7 Absorption and emission spectroscopy

Relevant information about aggregates can be obtained from absorption and emission spectra. The characterization of samples prior to doing time resolved experiments was done by steady state spectroscopy. Some general methods can be indicated.

The absorption spectra were recorded mostly using light from a tungsten filament lamp of 150 W. A few milliwatts of light intensity are sufficient for any absorption spectrum, so strong attenuation is necessary. Fluorescence excitation was mostly done by laser light, of either 514 nm argon–ion wavelength, or a tunable wavelength from a dye laser. For excitation spectra the light of the tungsten lamp was predispersed in a scanning monochromator. The resulting monochromatic light is used for fluorescence excitation.

After collimation the fluorescent emission is then focused on the entrance slit of a Spex1704 3/4 m monochromator. The resolution of the monochromator ranges from 0.5 cm^{-1} to 15 cm^{-1}, depending on the slit widths. The detectors used were photomultiplier tubes and photodiodes. For low light levels photomultipliers are the detectors of choice, the actual type of photomultiplier depends on the particular application. The red sensitive, low dark current tubes were only used in critical circumstances. More simple tubes were used for routine measurements. The photocurrent from the photomultiplier was converted into a voltage and consequently amplified. The amplifier was either a home–built stable DC amplifier, or a PAR128A lock–in with comparable signal–to–noise characteristics. The photodiode used to detect transmitted light was the silicon p-i-n diode of the Spectra–Physics power meter. The output of the amplifier was fed into a Hewlett–Packard chart recorder, and recorded on paper.

In a few cases integrated equipment was used. The Cary UV–VIS spectrometer was adapted to house a small cryostat, so some low temperature measurements were possible. The Spectroscopy Instruments/ Princeton Instruments Optical multichannel analyzer (OMA) was used on some occasions. The apparatus is ideal from a technological viewpoint. However, a bad integration of the detector with the necessary computer software limited its use during my experiments.

3.8 Sample preparation and handling

The aggregates that were studied formed from saturated monomer solutions. The equilibrium was shifted towards aggregation, by lowering the temperature, or by evaporating the solvent, or by increasing the concentration of anions. Most experiments were done at low temperatures where the systems are in the solid phase. Freezing the solutions is necessary in order to prevent any changes of the aggregates. In this section I will discuss some details of the kinetics of aggregate formation, preparation of solutions, and cryogenic sample handling.

Ever since Scheibe and Jelly published their separate papers [42,43] describing the formation of a narrow aggregate band in aquous PIC solutions, researchers have been interested in the process of the

aggregation. For the PIC case Scheibe himself was involved in settling most open questions, almost 40 years after his first paper was published [44]. The main elements in the description were: precipitation–like formation, a minimum stable aggregate size of seven units, and attachment of counterions to the aggregate. From osmometry and spectrometry it was concluded that aggregates behave like a heterogeneous equilibrium as that of any salt, with a solubility product constant $[Pic^+]\times[X^-]$ in the order of 10^{-4} at room temperature (X^- can be Cl^-, Br^-, I^-, F^-, SO_4^{2-}, CO_3^{2-}). The enthalpy of solvation for PIC–chloride aggregates was determined to be 30 kJ/mol. A nucleation step in the formation was identified; seven units are necessary to form a stable aggregate. One can imagine that the positively charged PIC cations show repulsive interactions. From osmometry it was concluded that most anions are bound to the aggregate. All of the observations show that the PIC aggregates are a stable phase between the solvated and the precipitated salt. Other dye molecules that form aggregates sometimes precipitate after standing for some time.

PIC solutions for low temperature measurements were prepared from ethylene glycol (Merck p.a.) and triply distilled water, mixed in a 1:1 ratio. This mixture was chosen for two reasons, the first being the extremely narrow J–bands that form at low temperature [45], and the second that the mixture has good glass forming properties. The concentrations were 1×10^{-2} M for PIC–Cl, 5×10^{-3} M for PIC–Br, and 2×10^{-3} M for PIC–I. In the room temperature solutions no aggregate formation occurred, showing that the solubility products are much higher than for aqueous solutions. Upon cooling the solutions to 77 K aggregation occurred. The extinctions reach values of over $10^5\,M^{-1}cm^{-1}$, so short path lengths of about 10 μm have to be used in order to keep the optical density below 1. Putting a small drop of solution between thin microscope glass plates gives rise to appropriate optical densities. The glass plates are mounted on a copper sample holder that is inserted in a conduction type cryostat that is at liquid nitrogen temperature (77 K).

The solvation product can be used to force aggregation by adding extra salt to the solutions. This scheme was used to make room temperature photon counting measurements on PIC water solutions. A mixture of 3×10^{-4} M PIC–Cl and 0.2 M KCl in water was gently heated to 50°C in order to get a monomer solution. The mixture was subsequently cooled to 20°C. A normal optical cuvette with a path length of 0.2 mm could now be used, without obtaining optical densities that were too high.

The experiments on TPY aggregates were done on samples of the dye in a polycarbonate matrix. The polycarbonate (PC) is rigid at room temperature, which facilitates handling. Solutions were made of 8 percent PC and 2.3 percent TPY–perchlorate (both by weight) in dimethylformamide. The solution was filtered carefully through a cellulose filter with pores of 0.2 μm. A drop of the solution was applied on a clean glass plate, and the glass plate was spun at a final speed of about 700 revolutions per minute for 45 seconds in a spincoat apparatus. The resulting polymer films varied in thickness from 1 to 4 μm, and had workable optical densities ranging from 0.1 to 1.0, depending on the precise procedures [46]. The films are blue and show the same spectrum as a dilute solution, implying that the dye is not aggregated. Aggregation is induced by exposing the films to saturated dichloromethane vapor. The polymer matrix

absorbs this vapor and the dye can associate, possibly enhanced by polymer crystallization which forces the dye molecules to move. Within thirty seconds the color of the film changes from blue to green. The films are dried and stored under vacuum in the dark until use. Polycarbonate is the only polymer in which TPY shows this strong aggregation, other polymers that can be spin coated like polymethylmethacrylate (PMMA) and poly(vinyl alcohol) (PVA) showed no aggregation. With the spincoat procedure also PIC aggregate films were made, PIC–Cl in PVA, PIC–Br and PIC–I in polycarbonate [47].

Samples of the thiacyanine dye (TD) aggregates were prepared according to a procedure similar to the one used with PIC. Solutions of 1×10^{-3} M TD in water/ethylene glycol 1:1 were made, KCl was added to a concentration of 0.1 M. At room temperature a color change from deep purple to bluish purple could be observed upon adding the salt. A drop was put between glass plates that were mounted on a sample holder.

The cooling process in the cryostat is rather critical. Immersing the solution samples of PIC and TD in liquid nitrogen does not result in aggregate formation, because cooling is too fast. The samples should be cooled to about –30°C for aggregation to take place, and after that cooled rapidly to below the solidification temperature at around –60°C. Putting samples in a conduction cryostat that is held at 80 to 100 K is sufficient to obtain the mentioned cooling conditions. In other cryostats procedures have to be adapted to meet aggregation and glass forming requirements.

Standard procedures are used to fill the cryostat with liquid helium in order to cool it down from 77 K to 1.5 K in about 45 minutes. The temperature is increased from 1.5 to 4.2 K by varying the helium pressure in the secondary helium reservoir. For temperatures above 4.2 K the sample can be heated by a resistor that is mounted on the sample holder. The thermal stability of the sample during a measurement is at its best when the whole cryostat slowly heats up without using any extra heating.

A small liquid nitrogen cryostat was used for some measurements inside the Cary UV/VIS absorption spectrometer, and also for some time resolved fluorescence experiments.

PIC–bromide was obtained from Exciton, PIC–iodide was obtained from Kodak, and PIC–chloride was prepared from the bromide salt by ion exchange over a column. TPY in the form of the perchlorate and tetrafluoroborate salt was a gift of Océ Nederland. The thiacyanine dye was donated by Polaroid USA.

References

1. W.H. Hesselink, Thesis University of Groningen, The Netherlands (1980).
2. W.H. Hesselink and D.A. Wiersma, Phys. Rev. Lett. **43**, 1991 (1979).
3. L.W. Molenkamp, Thesis University of Groningen, The Netherlands (1985).
4. W.R. Ware, in "Time–Resolved Fluorescence Spectroscopy in Biochemistry and Biology", eds. R.B. Cundall and R.E. Dale (Plenum Press, New York, 1983).

5. Z. Vardeny and J.Tauc, Opt. Comm. **39**, 396 (1981).
6. Y.R. Shen, "The Principles of Nonlinear Optics" (Wiley, New York, 1984)
7. Y.J. Yan and S. Mukamel, J. Chem. Phys. **89**, 5160 (1988), R. Boyd and S. Mukamel, Phys. Rev. A **29**, 1973 (1984).
8. R.L. Fork, C.H. Brito-Cruz, P.C. Becker and C.V. Shank, Opt. Lett. **12**, 483 (1987).
9. A. Asaka, M. Nakatsuka, M. Fujiwara and M. Matsuoka, Phys. Rev. A **29**, 2286 (1982).
10. N. Morita and T. Yajima, Phys, Rev. A **30**, 2525 (1984).
11. R. Beach and S.R. Hartmann, Phys. Rev. Lett. **53**, 663 (1984).
12. M. Tomita and M. Matsuoka, J. Opt. Soc. Am. B **3**, 560 (1986).
13. see: G.R. Fleming, "Chemical Applications of Ultrafast Spectroscopy" (Oxford University Press/ Clarendon Press, New York, 1986).
14. see: A.E. Siegman, "Lasers" (University Science Books, Mill Valley USA, 1986).
15. Coherent Inc. "Dye laser fact sheet".
16. J.J. Korperhoek, Research report, University of Groningen, (1990), J.J. Korpershoek, E.W. Castner and D.A. Wiersma, Opt. Comm. **78**, 90 (1990).
17. T.M. Bear and D.D. Smith. in "Ultrafast Phenomena IV", pg 96 (Springer, Berlin, 1984).
18. W.H. Hesselink and D.A. Wiersma, in "Modern Problems in Condensed Matter", Vol **4**, pg 249, Eds V.M. Agranovich and A.A. Marudin (North-Holland, Amsterdam, 1983).
19. L.W. Molenkamp and D.A. Wiersma, J. Chem. Phys. **80**, 3054, (1984).
20. W.H. Hesselink and D.A. Wiersma, J. Chem. Phys. **75**, 4192 (1981).
21. J.G. Fujimoto and T.Yee, IEEE J. Quantum Electr. **22**, 1215 (1986).
22. V.L. Vinetskii, N.V. Kukharev, S.G. Odulov and M.S. Soskin, Sov. Phys. Usp. **22**, 742 (1979).
23. M.J. Ehrlich, L.C. Phillips and J.W. Wagner, Rev. Sci. Instrum. **59**, 2390 (1988).
24. J.P. Heritage, Appl. Phys. Lett. **34**, 470 (1979).
25. Z.D. Popovic and E.R. Menzel, Chem. Phys. lett. **45**, 537 (1977).
26. P. Bado, S.B. Wilson and K.R. Wilson, Rev. Sci. Instrum. **53**, 706 (1982).
27. L. Andor, A. Lörincz, J. Siemion, D.D. Smith and S.A. Rice, Rev. Sci. Instrum. **55**, 64 (1984).
28. M. van Exter and A. Lagendijk, Rev. Sci. Instrum. **57**, 390 (1986).
29. G.R. Fleming, S.H. Courtney and M.W. Balk, J. Stat. Phys. **42**, 83 (1976).
30. E.W. Castner Jr., B. Bachi, M. Maroncelli, S.P. Webb, A.J. Ruggiero and G.R. Fleming, Ber. Bunsenges. Phys. Chem. **92**, 363 (1988).
31. M.A. Kahlow, W Jarzeba, T.P. DuBruil and P.F. Barbara, Rev. Sci. Instrum. **59**, 1098 (1988).
32. D. Bebelaar, Rev. Sci. Instrum. **50**, 1629 (1980).
33. M. Chang, S.H. Courtney, A.J. Cross, R.J. Gulotty, J.W. Petrich and G.R. Fleming, Anal. Instrum. **11**, 433 (1985).
34. D. Bebelaar, Rev. Sci. Instrum. **57**, 116 (1986).
35. K. Koyama, H. Kume and D. Fatlowitz, "Application of MCP-PMTs to Time Correlated Single Photon Counting and Related Procedures", Hamamatsu

Photonics K.K., Technical Information, No. ET-03/OCT 1987.
36. K.E. Drabe and J. Terpstra, private communication.
37. All programs were written by F. de Haan, information concerning these excellent programs can be obtained from: F. de Haan, Department of Physical Chemistry, Nijenborgh 16, 9747 AG Groningen.
38. D.V. O'Connor, W.R. Ware and J.C. Andre, J. Phys. Chem. **83**, 1333 (1979).
39. P.R. Bevington, "Data Reduction and Error Analysis for the Physical Sciences" (McGraw–Hill, New York, 1969).
40. W.H. Press, B.P Flannery, S.A. Teukolsky and W.T. Vetterling, recipes, the Art of Scientific Computing" (Cambridge Press, Cambridge, 1986).
41. A. Grinvald, Anal. Biochem. **75**, 260 (1976), A. Grinvald and I.Z. Steinberg, Anal. Biochem. **59**, 583 (1974).
42. G. Scheibe, Angew. Chem. **49**, 563 (1936), Angew. Chem. **50**, 51 (1937), Angew. Chem. **50**, 212 (1937).
43. E.E. Jelley, Nature **138**, 1009 (1936), Nature **139**, 631 (1937).
44. E. Daltrozzo, G. Scheibe, K. Gschwind and F. Haimerl, Photogr. Sci. Eng. **18**, 441 (1974).
45. W. Cooper, Chem. Phys. Lett. **7**, 73 (1970).
46. W. van Veenen, Research Report University of Groningen (1988).
47. M. Bosma, Research Report University of Groningen (1987).